SLAC-PUB-1081
ITP-415
(TH) and (EXP)
August 1972

THE EXTRACTION OF ASYMPTOTIC NUCLEON CROSS SECTIONS FROM DEUTERIUM DATA

W. B. Atwood*

Stanford Linear Accelerator Center

Stanford University, Stanford, California 94305

Geoffrey B. West**

Institute of Theoretical Physics, Department of Physics,

Stanford University, Stanford, California 94305

(Submitted to the XVI International Conference on High Energy Physics, Batavia, Illinois, Sept. 6-13, 1972. Also submitted to Phys. Rev.)

*Work supported by the U. S. Atomic Energy Commission

**Research sponsored by the Air Force Office of Scientific Research, Office of Aerospace Research, U. S. Air Force, under AFOSR Contract No. F44620-71-C-0044

ABSTRACT

The effect of Fermi motion on the extraction of asymptotic total neutron cross-sections from deuterium data is examined in some detail. Particular attention is paid to the threshold condition on the nucleon cross-sections. Using realistic hard-core wave functions to describe the deuteron, we find that, with this added correction, the Glauber mean inverse square radius of the deuteron is experimentally determined to be 0.0212 ± 0.005 mb^{-1} in good agreement with values calculated using hard-core wave functions. Previous discrepancies in πN and NN scattering are shown to be eliminated. When applied to the real photoabsorption total cross-section our correction considerably reduces the neutron-proton difference making it consistent with zero in the asymptotic region. We also examine deep inelastic electron-deuteron scattering and show how the theory gives an excellent description of the quasi-elastic peak. For scattering into the continuum we find that the correction far away from threshold is $\sim 5\%$, whilst near the threshold it can become very large ($\sim 30\%$). In terms of the neutron-proton ratio the correction is generally very small (i.e., the smeared ratio is an excellent approximation to the unsmeared) unless this ratio drops below $\sim 1/4$ near threshold.

Introduction

An important source of high energy interaction data relies on the accurate extraction of neutron cross sections from deuterium scattering measurements. Since the deuteron binding energy is small (~ 2.2 MeV) it is tempting, especially in the asymptotic region, to write the deuteron cross section (σ_d) as the sum of the free nucleon cross sections (σ_p, σ_n)

$$\sigma_d = \sigma_p + \sigma_n \tag{1}$$

Intuitively one does not expect the 2.2 MeV binding energy to be significant in a region where the energy scale is many GeV. However, it is generally well known that there are small, but important, corrections to this approximation, even in the asymptotic region where total cross-sections are essentially constant. Of these corrections only the Glauber correction [1], which arises physically from the shadowing of one nucleon by the other, has been given adequate attention. Its effect (to be discussed in Section III) tends to deplete total deuteron cross-sections by roughly 5%. This is the only correction which is usually made to Eq. (1) when extracting σ_n from σ_d.

Recently it has been suggested that there is another important, calculable correction to Eq. (1). [2] The origin of this correction stems from the fact that the bound nucleons undergo Fermi motion and are thus off of their mass shells. The qualitative features of this effect and its origin have been discussed in some detail in paper I [2] to which the reader is referred. The main effort of the present paper will be devoted to a quantitative evaluation of this "smearing" correction with emphasis on asymptotic cross-sections.

The fact that the target nucleons are moving affects the cross-sections in two distinct ways: 1) the total center of mass energy seen by the constituent nucleons is "doppler shifted;" and 2) the flux of incident particles in the rest frame of the moving nucleon is different from that in which the cross-section of free nucleons

is measured. If the free nucleon cross-sections are strongly energy dependent, the first effect could be expected to be large; this is the conventional smearing effect. If they are slowly varying, as they are at high energies, one would expect this effect to be negligible. In paper I we pointed out that there is a phase space restriction on the nucleon momentum due to the fact that the constituents are not free nucleons but bound nucleons; this can, and does, deplete σ_d. It is also found that the flux factor depletes σ_d relative to that of $(\sigma_n + \sigma_p)$. These effects depend crucially upon the distribution of nucleon momenta and in particular upon the tail of the distribution inside the deuteron. In Section III a quantitative calculation using conventional wave functions (see the Appendix) shows that these "smearing" effects can be of comparable importance to the shadow correction in the asymptotic region.

As emphasized in paper I, the Glauber effect is expected to be negligible in deep inelastic electron scattering, so that the smearing effects become the dominant calculable correction to the radiatively corrected deuteron data. In particular, near the inelastic threshold where the differential cross-sections are strongly S dependent our correction dominates the measured cross-section. We shall discuss this in detail in Section IV.

The plan of the paper is as follows: in Section II we briefly review the theory presented in paper I. In Section III we limit ourselves to the case where the mass of the incident particle is small and finite as in pion, nucleon, or real photon scattering. We find that the effective measured Glauber parameter $\langle r^{-2} \rangle$ is decreased by about 30%. Its magnitude ($0.0212 \pm .0066$ mb^{-1} in πN scattering and 0.0213 ± 0.0038 mb^{-1} in NN scattering) is consistent with $\langle r^{-2} \rangle \simeq .022$ calculated using "realistic" hard core wave functions, ("soft" wave functions such as the Hulthén give values of $\langle r^{-2} \rangle \gtrsim .0251$ mb^{-1}). In real photoabsorption we find that when

proper account is taken of this effect the difference between the neutron and proton cross-sections is considerably reduced and is consistent with zero. In Section IV we examine inelastic electron scattering and show that the theory gives an excellent description of the quasi-elastic scattering peak in deuterium. For scattering into the continuum our effect introduces large corrections to existing data in the important threshold region. We confirm the existence of a cross-over point (i.e., the point where the smearing correction to (1) changes sign) and show that it is essentially wave function independent. Finally, we present a calculation of the expected smeared neutron to proton ratio in deep inelastic electron cross-sections based upon various models for the unsmeared ratio. We find that the smeared ratio closely follows the unsmeared ratio except when the latter drops below $\sim 1/4$ near threshold. In such cases the smeared ratio remains relatively large although the unsmeared ratio can become vanishingly small.

Note that we have used conventional hard-core wave functions throughout in describing the deuteron momentum distributions. This is discussed in the Appendix where we give details of the wave functions used and discuss their applicability to the present problem.

II. THEORY

This Section contains a review of the results of paper I. We shall present the results in two cases: a) where the incident particle has a small but finite mass; and (b) where the incident particle has a virtual mass which can become large (as in electron scattering). In part (c) we discuss the identification of the virtual scattering amplitudes.

A. Hadronic Scattering and Total Photoabsorption

The analysis is based upon an incoherent impulse approximation (for a review of the corrections to this the reader is referred to paper I). This approximation excludes shadowing corrections. We shall discuss these in Section III.4. The square of the deuteron scattering matrix elements is simply written as the sum

of the squares of the corresponding nucleon scattering matrix elements. In terms of Feynman graphs the process is approximated by the graph shown in Fig. 1. We thus have

$$|T|^2 = \int \frac{d^3 p_s}{(E_s/M)} \; |f(\underset{\sim}{p}_s)|^2 \left[|T_n|^2 + |T_p|^2 \right] \tag{2}$$

where the $|T|^2$ represent the squares of the T matrix elements suitably summed and averaged over initial and final states; $|f(\underset{\sim}{p}_s)|^2$ is the probability that a particular nucleon has momentum $\underset{\sim}{p}_s$ in the rest system of the deuteron; $E_s = \sqrt{\underset{\sim}{p}_s^2 + M^2}$ is the energy of the spectator nucleon and M is the nucleon mass; $f(\underset{\sim}{p}_s)$ is simply the Fourier transform of the deuteron spatial wave function. Ambiguities arise in identifying the non-relativistic wave-functions found in the literature with the relativistic case used here. In particular, we choose the following normalization: (this is discussed in the Appendix).

$$\frac{f(\underset{\sim}{p}_s)}{E_s/M} = \left[U_p(\underset{\sim}{p}_s)^2 + W_p(\underset{\sim}{p}_s)^2 \right]^{1/2} \tag{3}$$

The S-wave transform is

$$U_p(\underset{\sim}{p}_s) = \sqrt{\frac{1}{2\pi^2}} \int_0^\infty \frac{u(r)}{r} \; j_o \; (|\underset{\sim}{p}_s| \; r) \; r^2 dr \tag{4a}$$

and the D-wave transform is given by

$$W_p \; (\underset{\sim}{p}_s) = \sqrt{\frac{1}{2\pi^2}} \int_0^\infty \frac{w(r)}{r} \; j_2 \; (|\underset{\sim}{p}_s| \; r) \; r^2 dr \tag{4b}$$

By introducing into Eq. (2) the usual flux factors which take matrix elements into cross-sections we can write (in the deuteron laboratory system)

$$\sigma_d = \int \frac{d^3 p_s}{(E_s/M)} \; |f(\underset{\sim}{p}_s)|^2 \left[\frac{\nu'^2 - q^2}{q^2} \right]^{1/2} (\sigma_n + \sigma_p) \tag{5}$$

where $\nu' \equiv \frac{p \cdot q}{M}$ with p the 4-momentum of the struck nucleon and q that of an incident particle of mass M_i and energy $E_i = q^o$. We shall parameterize the σ's in terms of the relevant total center of mass energies of the incident particle-nucleon system: for a nucleon at rest (on shell)

$$S = M^2 + 2ME_i + M_i^2$$

whilst for an interacting nucleon (off shell)

$$S' = (p + q)^2$$
$$= p^{o2} - \underset{\sim}{p}_s^2 + 2M\nu' + M_i^2$$

We thus obtain

$$\sigma_d(S) = \frac{\pi}{2q^2M} \int_0^\infty \frac{|\underset{\sim}{p}_s| d p_s}{E_s/M} |f(\underset{\sim}{p}_s)|^2 \int_{S_-}^{S_+} dS' \eta \left[\sigma_p(S') + \sigma_n(S')\right]$$

Where $\eta = \left[(S' - M_i^2 - M_d^2 - M^2 + 2M_d E_s)^2 - 4M^2 M_i^2\right]^{1/2}$ (6)

and $S'_\pm = M_i^2 + M_d^2 + M^2 + 2\left[q^o (M_d - M_s) - M_d E_s\right] \pm 2 |\underset{\sim}{q}| |\underset{\sim}{p}_s|$

Physically η represents the covariant flux factor relating $|T|^2$ to σ. It should be emphasized that there is a further restriction on the S' integration coming from the threshold condition on $\sigma(S')$, i.e., $\sigma(S') = 0$ when $S' < M^2$. This is discussed in detail in paper I. We shall generally work in the laboratory (LAB) system where the four-momentum of the deuteron is $P_d = (M_d, \underset{\sim}{0})$ so that $\underset{\sim}{p}_s + \underset{\sim}{p} = \underset{\sim}{0}$. Note that this implies that the energy of the interacting nucleon is

$$p^o = M_d - E_s = M_d - \sqrt{\underset{\sim}{p}_s^2 + M^2} \qquad (7)$$

Equation (6) is the basis for our calculation of the correction for both purely hadronic and real photon scattering. We shall parameterize the correction by a

parameter β (S) which is defined by

$$\sigma_d(S) = (\sigma_n(S)) + \sigma_p(S)) \ (1 - \beta(S))$$

so if $\sigma_p \simeq \sigma_n$ (8)

$$\beta(S) = 1 - \frac{\sigma(\text{SMEARED})}{\sigma}$$

β(S) is to be calculated from Eq. (6). We shall discuss this further in Section III below.

B. Electroproduction

In the one photon exchange approximation (see Fig. 2) the electromagnetic structure of the target can be described by the Lorentz covariant tensor[3].

$$W_{\mu\nu} = 1/2 \sum_N <p|j_\mu| N><N|j_\nu|p> (2\pi)^3 \ ^4\delta(P_N - p - q) \quad (9)$$

where j_μ is the electromagnetic current operator, p the four-momentum of the target and the sum includes an average over the initial particle spin. Here q represents the four-momentum of the incident virtual photon. The most general form for $W_{\mu\nu}$ consistent with Lorentz covariance, gauge invariance and conservation of parity is

$$W_{\mu\nu} = -W_1(\nu, q^2)\left(g_{\mu\nu} - \frac{q_\mu q_\nu}{q^2}\right) + \frac{W_2(q^2, \nu)}{M^2}\left(p_\mu - \frac{M\nu}{q^2} q_\mu\right)\left(p_\nu - \frac{M\nu}{q^2} q_\nu\right) \quad (10)$$

where $\nu = p\cdot q/M = \frac{S-M^2-q^2}{M}$ and the W_i are scalar functions of the independent variables q^2 and ν (and in principle p^2; for a free target p^2 is of course fixed). Sometimes we shall choose the variables q^2 and S rather than q^2 and ν. In terms of these W_i the doubly differential cross section is

$$\frac{\partial^2\sigma}{\partial\Omega\partial E'} = \frac{4\alpha^2}{q^4} E'^2 \cos^2(\theta/2)\left[W_2 + 2W_1 \tan^2(\theta/2)\right] \quad (11)$$

where E' is the energy of the scattered electron, Θ its scattering angle (in the LAB.) and $d\Omega$ the elemental solid angle; α is the fine structure constant ($\simeq 1/137$). The analogous equation to Eq. (2) for the scattering from the nucleons bound in deuterium is

$$W^d_{\mu\nu} = \int \frac{d^3p_s}{E_s/M} \; |f(p_s)|^2 \left[W^p_{\mu\nu} + W^n_{\mu\nu} \right] \tag{12}$$

If the z-axis is defined to be along the direction of the virtual photon, an examination of the various tensorial components leads to the following equations

$$W^d_1(q^2, \nu) = \int \frac{d^3p_s}{E_s/M} \; |f(p_s)|^2 \left[W^p_1(q^2, \nu') + W^n_1(q^2, \nu') + \frac{p_x^2}{M^2} \left| W^p_2(q^2, \nu') + W^n_2(q^2, \nu') \right| \right] \tag{13a}$$

$$W^d_2(q^2, \nu) = \int \frac{d^3p_s}{E_s/M} \; |f(p_s)|^2 \left[\left(\frac{\nu'}{\nu}\right)^2 \left\{ \left(1 - \frac{p_z q^2}{M\nu' |\vec{q}|} \right)^2 - \frac{p_x^2}{M^2} \frac{\nu^2}{\nu'^2} \frac{q^2}{\vec{q}^2} \right\} \left| W^p_2(\nu', q^2) + W^n_2(\nu', q^2) \right| \right] \tag{13b}$$

These can easily be reduced to a form analogous to Eq. (6). Again, we remind the reader that implicit in the definition of the W_i is the constraint that they vanish below threshold, i.e., for $S' < M^2$.

C. Identification of Virtual Particle Cross-Sections

In both electromagnetic and strong interaction scattering an ambiguity arises as to what one should use for the total cross-sections for scattering from a virtual particle. Although we shall assume that these are the same as the real particle total cross-sections there is nevertheless the problem as to which is the most

convenient or relevant variable (e.g., S or ν). We shall now present a threshold argument [4] for choosing a particular variable.

In writing Eq. (13) we have used the conventional variables q^2 and ν. However, suppose we artificially separate W_2 into an elastic and inelastic contribution.

$$W_2 = W_2^{\text{elastic}} \; \delta \; (p + q)^2 - M^2) + W_2^{\text{inelastic}} \; \Theta \; [(p+q)^2 - M_{th}^2] \qquad (14)$$

where the pion threshold is $M_{th} = M + M_\pi$. Now if the nucleon is free, the argument of the δ-function is

$$(p+q)^2 - M^2 = q^2 + 2p \cdot q \qquad (15)$$

whilst, if it is virtual, the argument is

$$(p+q)^2 - M^2 = q^2 + 2p \cdot q + p^2 - M^2 \qquad (16)$$

If we define

$$\widetilde{\nu} \equiv \frac{p \cdot q}{M} + \frac{p^2 - M^2}{2M} \qquad (17)$$

then Eqs. (15) and (16) have the same form (i.e., $q^2 + 2\,\widetilde{\nu}\,M$) in the two cases. The same result follows for the argument of the Θ - function. Hence in order to ensure the correct threshold behavior in a simple way, it is obviously convenient to consider the W 's as functions of q^2 and $\widetilde{\nu}$. Equivalently one could, of course, consider them as functions of q^2 and S from the outset and avoid the threshold problem entirely. Both sets of variables have been used in evaluating the smearing.

As an example, consider the large $q^2 (-q^2 > 1\ (\text{GeV/c})^2$ behavior of νW_2; experimentally this function scales, i.e., it becomes a function of the single

variable $\omega = -2M\nu/q^2$:

$$\nu W_2(q^2, \nu) \to F_2(\omega) \tag{18}$$

In terms of the ω variable, the threshold for $F_2(\omega)$ for an on-shell nucleon occurs at $\omega = 1$. However, when the nucleon is off-shell the threshold occurs at $\omega = 1 + (p^2 - M^2)/q^2$. There is nothing wrong with this; however, it is rather more convenient (and aesthetic) if we can maintain the threshold value of the scaling variable at $\omega = 1$. Choosing the $\omega = 1$ threshold and not the physical threshold for the interacting nucleon leads to a smeared cross section which is $\sim 2\%$ larger. Throughout this work we have used the (S', q^2) variables rather than the conventional (ν', q^2) using the threshold condition $S' < M^2 \Rightarrow F_2(\omega) = 0$.

III. STRONG INTERACTION EFFECTS AND PHOTOPRODUCTION

In this section we apply the results of Section II to both strong interaction and total photoabsorption cross sections at high energies. We first discuss the role of the Glauber shadow correction and show how the Doppler effect changes the apparent size of the measured mean inverse square radius of the deuteron, $\langle r^{-2} \rangle$. We then show that in photoabsorption this new effect implies that the asymptotic neutron and proton cross sections are equal within errors.

A. Glauber Effect

The conventional Glauber shadow correction to Eq. (1) is of the form

$$\sigma_d = \sigma_p + \sigma_n - \frac{\langle r^{-2} \rangle}{4\pi} \sigma_p^2 \tag{19}$$

where, in the correction term, we have set $\sigma_n = \sigma_p$. We assume that the scattering amplitudes for neutrons and protons are purely imaginary. The energy independent

parameter is given by [1]

$$\langle r^{-2} \rangle = 1/2 \int_0^\infty F_d(t) \frac{f_p(t)}{f_p(0)} \frac{f_n(t)}{f_n(0)} dt \tag{20}$$

where f(t) is the scattering amplitude for elastic scattering from the nucleon ($\sim e^{-bt}$ with $b \sim 9.6\,(\mathrm{GeV/c})^{-2}$) which is taken to be energy independent. $F_d(t)$ is the conventional deuteron elastic form factor defined by

$$F_d(q^2) = \int e^{i \underset{\sim}{q} \cdot \underset{\sim}{r}} |\psi(r)|^2 d^3r \tag{21}$$

where $\psi(r)$ is the deuteron wave function. There are two cases where <u>all</u> the relevant cross sections occuring in Eq. (19) can be measured: (i) pion nucleon scattering (whereby isospin invariance $\sigma_{\pi^+ p} = \sigma_{\pi^- n}$) and (ii) nucleon-nucleon scattering where σ_{np} can be measured. In practice we can, therefore, check Eq. (20) directly: the quantity

$$\langle r^{-2} \rangle_o = 4\pi \frac{\sigma_p + \sigma_n - \sigma_d}{\sigma_p^2} \tag{22}$$

can be measured and checked against Eq. (20). However, our correction adds a new term to the right hand side of Eq. (19) which now takes the form

$$\sigma_d = \sigma_p + \sigma_n - \frac{\langle r^{-2} \rangle}{4\pi} \sigma_p^2 - 2\beta(S)\, \sigma_p \tag{23}$$

where $\beta(s)$ is to be calculated from Eq. (6). This can be reexpressed as

$$\langle r^{-2} \rangle = \langle r^{-2} \rangle_o - \frac{8\pi\, \beta(S)}{\sigma_p} \tag{24}$$

showing explicitly that $<r^{-2}>$ will always appear larger than its actual value if the "smearing" effect is neglected.

B. Determination of $<r^{-2}>$ from Experiment

We have used Eq. (6) to evaluate $\beta(S)$ using various wave functions combined with fits to a variety of data. The results are shown in Fig. 3 and Table I [5]. The shape of $\beta(S)$ is essentially wave function and process independent (Fig. 3 shows the results calculated for photoproduction) whereas its magnitude is rather strongly dependent upon the wave function. As explained in I this is to be expected since β is sensitive to the tail of the momentum distribution and this varies considerably from one wave function to another. The fact that β is process independent merely reflects the fact that total cross sections have similar shapes in the asymptotic region. Using values of β calculated by making fits to the experimental data we have attempted to estimate $<r^{-2}>$ from Eq. (24) using πN and NN data. A basic problem here occurs in the evaluation of $<r^{-2}>_0$ from the data using the definition (22) since we obviously have to combine different experiments in different energy regions.

In Table I we present the calculated values of $<r^{-2}>$ and $\beta(S)$ for different wave functions for NN scattering at $E_i = 10$ GeV. In doing so, we have assumed that $\sigma_{pn} = \sigma_{pp}$ which is borne out by the data [5f, 5g]. The values of $\beta(S)$ quoted at 10 GeV for the NN case are a good estimate (within $\pm$ 5%) of the values in πN as well as NN with $S > 4$ GeV^2 cases. It is also interesting to note that for the cases where the estimated correction is small (due to wave functions with smaller high momentum tails) the corresponding values of $<r^{-2}>$ calculated from Eq. (20) increase. The resulting compensation means that the combined effect of the two corrections is roughly equivalent to taking $<r^{-2}>_0$ to be .03 mb^{-1} as is usually done by the experimentalists!

In Table II various values of $<r^{-2}>$ and $<r^{-2}>_0$ are shown calculated from experiment. The errors shown are purely statistical. These errors are misleading due to the presence of large systematic errors. For example, one can easily estimate the systematic error due to uncertainties in target densities. In particular, the liquid deuterium density is known only to $\pm .6\%$ [6]. This uncertainty by itself, assuming no error in measuring the vapor pressure, results in systematic uncertainties of .0065 mb^{-1} for πN and .0040 mb^{-1} for NN. This crude estimate is probably at least a factor of two too conservative for the overall systematic error in the actual experimental situations (i.e., $\Delta\rho_d/\rho_d \simeq 1.0\%$). For this reason alone the NN and πN data can not be considered as a rigorous test of the theory.

C. $\sigma_p - \sigma_n$ in Photoproduction

We now turn our attention to the photoproduction cross sections. As in the hadronic case, only a shadowing correction has been made to the deuterium data when extracting the neutron cross section.[7] In this case shadowing is complicated by the fact that inside the nucleus the photon can behave like a hadron. Several authors have investigated this problem using the vector dominance approximation, and we have simply followed the procedure used by the experimentalists, namely the work of Brodsky and Pumplin.[8] As before, we can write

$$\sigma_{\gamma n} = \sigma_{\gamma d} - \sigma_{\gamma p} + 2\beta\,\sigma_{\gamma p} + (GC) \tag{25}$$

where GC is the Glauber correction which we take from Ref. 7. Our results are expressed in the form $\sigma_p - \sigma_n$ and are shown in Fig. 4. They show that the difference is asymptotically consistent with zero and approaches it considerably faster than without our correction. We have shown the results only for the Hamada-Johnston wave function, but the results for the others can be estimated by using the plots

of β in Fig. 3. We have also attempted to fit the difference by the expected Regge asymptotic forms (Pomeron + A_2 - exchange)

$$\sigma_{\gamma p} - \sigma_{\gamma n} = A + B\ \nu^{-1/2} \tag{26a}$$

$$= A + B\ S^{-1/2} \tag{26b}$$

The results are shown in Table III. It is clear that the combined errors are sufficiently large that it is very difficult to draw any definitive conclusions. We should also mention that the values of the fit parameters are sensitive to the cut-off in small W. We have chosen to take points for which $W > 1.9$ GeV.

IV. INELASTIC ELECTRON SCATTERING

A. Quasi-Elastic Scattering

Quasi-elastic scattering is defined by the constraint that the interacting nucleon emerges on its mass shell; in other words, in this special case, $S' = (p+q)^2 = M^2$. The scattering from the nucleons can thus be expressed in terms of the conventional elastic nucleon form factors $G_E(q^2)$ and $G_M(q^2)$. It is not difficult to show that nuclear structure functions now take the form:

$$W_1(q^2, S) = \frac{-q^2}{2M} G_M^2(q^2)\, \delta\left[(p+q)^2 - M^2 \right] \tag{27a}$$

$$\equiv G_1(q^2)\, \delta(S - M^2)$$

and

$$W_2(q^2, S) = 2M \left[\frac{G_E^2 - \frac{q^2}{4M} G_M^2}{1 - q^2/4M^2} \right] \delta\left[(p+q)^2 - M^2 \right]$$

$$\equiv G_2(q^2)\, \delta(S - M^2) \tag{27b}$$

These are to be inserted into Eq. (13). The δ function allows one of the integrals to be performed trivially. It turns out to be most convenient to use the center-of-mass

system of the outgoing nucleons in order to perform the calculations. We shall employ a tilde to denote variables measured in that system. We find

$$W_2^{SMEARED} = \frac{\pi \tilde{p}_s}{2\sqrt{S_t}} G_2(q^2) \int_{-1}^{+1} \mathscr{T} |f(p_s)|^2 \, d\cos\tilde{\Theta} \tag{28a}$$

$$W_1^{SMEARED} = \frac{\pi \tilde{p}_s}{2\sqrt{S_t}} G_1(q^2) \int_{-1}^{+1} |f(p_s)|^2 \, d\cos\tilde{\Theta} + \tag{28b}$$

$$+ \frac{\pi \tilde{p}_s}{2\sqrt{S_t}} G_2(q^2) \int_{-1}^{+1} \frac{p_x^2}{M^2} |f(p_s)|^2 \, d\cos\tilde{\Theta}$$

where

$$S_t = (P_d + q)^2 \quad ; \quad \tilde{p}_s = \sqrt{\tfrac{1}{4} S_t - M^2}$$

and by Lorentz transforming the longitudinal and transverse parts of the momentum

$$p_x^2 = 1/2\, p_\perp^2 = 1/2\, \tilde{p}_s^2 (1 - \cos^2\tilde{\Theta})$$

$$p_s^2 = \tilde{p}_s \cos\tilde{\Theta} \frac{(M_d - \nu)}{\sqrt{S_t}} - \frac{q \tilde{E}_s}{\sqrt{S_t}}$$

$$p_s^2 = 2p_x^2 + p_z^2$$

since $p_x^2 = p_y^2$ by azimuthal symmetry. Finally, $\mathscr{T}$, the tensor term for W_2 smearing, is given by

$$\mathscr{T} = \frac{1}{M^2} \left[(p^o - \frac{\nu}{q} p_z)^2 + (1 - \frac{\nu^2}{q^2}) p_x^2 \right]$$

where

$$p^o = M_D - E_S$$

An extensive comparison of this theory with experimental data[9a] has been made. Figure 5 shows an example for $\Theta = 4^o$ and $E_o = 16$ GeV. The data used[9a] has not been radiatively corrected, so we have made our

comparison by performing radiative correction to our theory, which is shown by the solid line in the figure. The fit is clearly an excellent one. Different wave functions yield only a very small change to the fit ($\leq 2\%$); indeed, they are sufficiently small to be comparable to corrections due to the finite n-p mass difference!

Previous theories[10] are equivalent to setting $\mathcal{F}=1$ in Eq. (28a) and dropping the second term from the R.H.S. of Eq. (28b). This suppression of the tensor terms, whose presence is required by gauge invariance, results in raising the low missing mass tail and lowering the high missing mass tail. Although the data does not yield positive proof for the presence of these tensor terms, they do improve agreement between experiment and theory.

Final state interactions and n-p interference terms have been neglected in the present calculation. The final state corrections are expected to be of diminishing importance as the incident energy and angle are increased (i.e., as $-q^2$ is increased). Their effect is to deplete the peak and fill in the low missing mass tail. Only at incident energies less than 7 GeV at $\Theta = 4^\circ$ was the presence of final state interactions very noticeable. Yet even here, integrals over the theory and the data were in good agreement. The n-p interference term also goes away very quickly with increasing $(-q^2)$. Thus, at high incident energies and/or large scattering angles, it is valid to neglect these effects and make a direct comparison. A similar agreement was obtained for energies 7-20 GeV. Furthermore, the 10° data[9b] was checked and found to be in good agreement with this theory, although the errors on this data were larger.

Two final remarks concerning the quasi-elastic calculation: First, only the elastic radiative deuteron tail peak was included. The elastic peak itself was not included. It also fills in the low missing mass tail when appropriately broadened

by the resolution. Secondly, smearing from the N* (1238) is seen to raise high missing mass data above the theory starting at 1.00 GeV. Incoherent pion production starting at pion threshold (W = 1.072 GeV) also smears down to W = 1.00 GeV.

B. Deep Inelastic Electron Scattering

Recent deep inelastic scattering results in the region $S \geq 4$ GeV^2, $-q^2 \geq 1$ (GeV/c)^2 indicate that the neutron structure functions differ from those of the proton.[3] In this subsection, we shall investigate this in some detail using the standard wave functions described in Appendix A. Using phenomenological fits to $F_2 = \nu W_2$ for the proton we have evaluated the ratio $F_2/"F_2"$; by "F_2" we mean the smeared value of F_2 given by Eq. (13). We made fits to the data in using both the ω and ω' variables[11] (for various values of q^2). The results are shown in Fig. 6a-6b. It should be pointed out that the smearing integrals depend on the nuclear structure functions from threshold up to a value of approximately twice that at which the smeared structure function is being calculated. Thus, if the fits of F_2 do not represent the data well over the entire region, it is possible for large discrepancies to arise. In particular, the ω fit is a relatively poor fit to the data, even in an average sense, whereas the ω' fit averages the data below $\sqrt{S} \sim 1.8$ GeV[11] and is a more realistic representation. Indeed we have found that if the data itself is used directly rather than a fit, the results are in agreement with those using the ω' fit, whereas the ω fit is in some disagreement for $2.0 \text{ GeV} \leq W \leq 2.4$ GeV.

From Fig.6, we see that the correction is relatively small in the large ω region, but grows rapidly near threshold ($W \leq 2$). This is to be expected from the general arguments given in I. In Fig. 6 we have plotted the ratio for various values of q^2 in order to illustrate the rather weak q^2 dependence of the correction; each q^2 line stops at a W of 2.0 (1.8) GeV for the ω (ω') fits. We have also investigated the wave function dependence; for the class of wave functions we have used, this is also

found to be relatively weak (see Fig. 7) (the Hamada-Johnston wave functions also lie right on top of the others).

An interesting way of representing the data is via the ratio

$$\rho = \frac{N(\text{SMEARED})}{P(\text{SMEARED})}$$

where by N (smeared) we mean "F_2" for the neutron (and similarly for the proton). The quantity of theoretical interest is, of course,

$$\rho' = \frac{N}{P}$$

(i.e., the unsmeared ratio). However, it might be hoped that the effects of smearing roughly cancel in the ratio. This ratio is of particular importance in quark parton models where it must remain greater than 1/4. We have investigated this possibility by choosing various simple models for ρ', using Eq. (13) to generate ρ. The results are shown in Fig. 8. If ρ never drops below 1/4, then ρ is a good, if not excellent, approximation to ρ'. On the other hand, if ρ does drop below 1/4, then the extraction of the correct ratio becomes a difficult problem. Recent experimental results indicate $\rho > 0.35$ in which case, the true ratio can probably be determined by simply setting $\rho = \rho'$.

Conclusion

In this paper we have examined in detail the quantitative effects of Fermi motion upon the extraction of asymptotic total neutron cross section using the theory of paper I. Combined with the Glauber shadowing correction, we are able to give an adequate account of πd, Nd, and γd scattering. This can be seen from Table II, where we show that average values of $\langle r^{-2} \rangle$ are consistent with values estimated from Glauber theory, Eq. (20). Table III shows the results for γd scattering. There are naturally large errors implicit in the data (statistical errors, errors coming from using different experimental data and sytematic experimental errors), so the conclusions should not be taken as complete. Furthermore, as already

emphasized [2], there are unknown contributions in the theory which cannot be estimated. An example of this is the use of non-relativistic wave functions in a region where relativity might be expected to play a role ($|\underline{p}_s| \sim 1$ GeV/c); this is briefly discussed in the Appendix. Another problem is associated with the fact that in the finite incident mass case (e.g., π-N scattering), the region which contributes to the depletion of σ_d due to the phase space restriction corresponds to the interacting nucleon being far off-mass-shell(~ 1 GeV^2). One might even question, in that case the whole description of a deuteron as a bound state of two nucleons.[13] There is no obvious way of correctly taking account of such difficulties and we have generally taken the philosophy that in some sense a hardcore wave function "mocks" up our ignorance of the short distance behavior in the deuteron. In any case, the effect is certainly present and estimable; whether it is possible that some subtle off-shell phenomenon or higher order scattering could compensate for the effect is certainly an open question. On the other hand, as has been emphasized in I, the origin of the effect is, like the Glauber effect, to be found in very simple physical phenomena, namely the Doppler effect and the threshold constraint on total cross sections; as such, a compensation is highly unlikely.

As $\omega \sim 1$ (i.e., threshold) in deep inelastic e-d scattering the sensitive region of the wave function corresponds to an interacting nucleon which comes nearer and nearer its mass shell (e.g., at $\omega = 2$: $p^2/M^2 = 2/3$). We might, therefore, expect any ambiguity due to off-shell effects to be of considerably less importance for small ω. This is important because this is the region where our effect is largest. We have shown that although the effect is large, the ratio N/P remains unchanged when smeared except when it falls below $\sim 1/4$ near threshold.

Finally, we should emphasize a point made in I, namely that should there be any anomalously large tail to $f(\underline{p}_s)$, then the effects will be drastically increased.

Conversely, should there be an anomalously small tail to $f(p_s)$, the effects would become negligible. It might therefore be hoped that eventually such experiments could yield useful information on the short distance behavior of the deuteron.

We thank our colleagues at Stanford for many helpful and stimulating discussions. The support of Group A in the numerical calculation and making available electroproduction data is gratefully acknowledged. One of us (WBA) in particular thanks A. Bodek for many useful discussions and critical comment throughout this work.

APPENDIX

Deuteron Wave Function

A non-trivial problem arises in the present theory in choosing the "correct" normalized relativistic momentum distribution $\phi(\underline{p}_s)|^2 = \frac{M}{E_s} f(\underline{p}_s)^2$. In practice, the non-relativistic wave functions were assumed to give an adequate approximation. Four such wave functions are shown in Fig. 9, where we have plotted $\phi(\underline{p}_s)$. These wave functions have been adjusted to fit phase shifts out to momenta of ~350 MeV/c, whereas the phase space effect discussed in this paper is sensitive to momenta ~750 MeV/c[2]. We thus need to extrapolate these wave functions out to momenta ~1-2 GeV/c. Whether this is realistic or not is far from clear. As an example, one might worry whether the (M/E_s) factor should be included explicitly in the wave function so that $f(\underline{p}_s)$ rather than $\phi(\underline{p}_s)$ is to be identified with its non-relativistic form. If one does drop this factor, then a typical smearing ratio σ/σ(smeared) changes by ~2%. We would argue that since the wave function is "fitted" to quasi-relativistic data, the more sensible choice is to identify $\phi(\underline{p}_s)$ with the usual wave function. This hardly resolves the problem, but at least motivates a particular choice.

Three of the wave functions used were of the "hard core" type: Lomon-Feshbach, Reid Hard Core, and Hamada Johnston (used everywhere except as noted). "Hard core" simply means that the spatial wave function is sharply cut off at some finite value of r (usually ~.5 fermi). This sharp edge introduces highly oscillatory high momentum components in the fourier transform of the spatial wave function. A realistic soft core wave function was also used: The Reid Soft Core. As seen in Fig. 9, its high momentum tail is considerably attenuated from that of the hard-core types. This soft core wave function shows the largest effect in β(S) (typically $\beta \simeq .011$ for the Reid Soft Core). Thus the soft core wave functions have their

largest deviations from hard core types where difference quantities near zero are calculated (i.e., the Glauber parameter $<r^{-2}>$ and $\sigma_p - \sigma_n$ in photoproduction). We emphasize that although there is a discernable effect here, it moves the data in all cases by less than a standard deviation.

REFERENCES

1. R.J. Glauber, Phys. Rev. 100, 242 (1955); V. Franco and R.J. Glauber, Ibid. 142, 1195 (1966).
2. G. B. West, Phys. Letters 37B, 509 (1971), and Ann. Phys. (N. Y.) to be published. These papers will be referred to as I.
3. For a review of the literature see, for example, the talk of H. Kendall in the Proceedings of the 5th International Symposium on Electron and Photon Interactions at High Energies, Cornell University, 1971.
4. This argument is based upon a suggestion by A. Bodek whom we thank (private communication).
5. The data we have used are the following:
   (a) W. Galbraith et al., Phys. Rev. 138, B913 (1965)
   (b) K.J. Foley et al., Phys. Rev. Letters 19, 330 (1967)
   (c) S. P. Denisov et al., Phys. Letters 36B, 415 (1971)
   (d) J.V. Allaby et al., Phys. Letters 30B, 500 (1969)
   (e) D.V. Bugg et al., Phys. Rev. 146, 980 (1966)
   (f) J. Engler et al., Phys. Letters 31B, 669 (1970)
   (g) L.W. Jones et al., Phys. Letters 36B 509 (1971)
   (h) NN and ND Interactions above .5 GeV- A Compilation Particle Data Group ed. O. Benary et al., UCRL-20000 NN 1970
6. Bubble Chamber Group Selected Cryogenic Data Notebook, ed. J.E. Jensen et al. BNL-10200, Brookhaven National Laboratory (November 1966).
7. D.O. Caldwell et al., Phys. Rev. Letters 25, 609 and 613 (1970); T.A. Armstrong et al., Daresbury preprint, DNPL/P 105 (1972).
8. See, e.g., S. J. Brodsky and J. Pumplin, Phys. Rev. 182, 1794 (1969).

9. (a) Quasi-elastic deuterium data courtesy of S. L. A. C. -Group A. (to be published (Experiment no. E-61))

(b) S. L. A. C. -MIT Collaboration (Experiment no. E-49a)

10. See, e.g., L. Durand. Phys. Rev. 115, 1020 (1959) and Phys. Rev. 123, 1393 (1961).

11. E. Bloom and F. Gilman, Phys. Rev. Letters 25, 1140 (1970).

12. The four deuteron wave functions used are:

(a) E. Lomon and H. Feshbach, Annals of Phys. 48, 94 (1968)

(b) T. Hamada and I. D. Johnston, Nuclear Physics 34, 382 (1962)

(c) R. V. Reid, Jr., Annals of Phys. 50, 411 (1968)

(d) Hulthén wave function: $u(r) = N^{-\alpha r}(1 - e^{-\lambda r})$, $\alpha = .232 f^{-1}$ $\lambda = 1.21\ f^{-1}$; and a "hard core" version: $u(r) = N'^{-\alpha r}(1 - e^{-\gamma r})^3$, $\gamma = 2.21 f^{-1}$.

13. This is the attitude taken by Lomon and Feshbach (ref. 12) and explained to us by H. P. Noyes (private communication).

TABLE I

Values of the parameters $<r^{-2}>$ and β for various wave functions[12]; β was evaluated for the p-p total cross-section at an incident energy of 10 GeV.

Wave Function	$<r^{-2}>(mb^{-1})$	β (E_i = 10 GeV)
Hamada-Johnston	.02220	.0140
Reid Hard Core	.02239	.0140
Reid Soft Core	.02244	.0117
Hulthén	.02507	.00814
Hulthén "hard core"	.02397	.00756

TABLE II

Values of $\langle r^{-2}_{o} \rangle$ and $\langle r^{-2} \rangle$ for various interactions (the errors quoted are only statistical-see text for an estimate of the systematic errors)

CASE	REFERENCE	E_i range (GeV)	$\langle r^{-2}_{o} \rangle$ (mb^{-1})	$\langle r^{-2} \rangle$ (mb^{-1})
1) π - N	5a	6 - 20	.0411 ± .0040	.0278 ± .0040
2) π - N	5c, 5d	20 - 60	.0271 ± .0029	.0128 ± .0026
3) π - N	5a, 5b	8 - 20	.0556 ± .0038	.0424 ± .0038
4) π - N	5b, 5c	15 - 20	.0346 ± .0006	.0210 ± .0006
5) N - N	5e	5 - 8	.0143 ± .0002	.0104 ± .0003
6) N - N	5a	6 - 22	.0348 ± .0044	.0268 ± .0044
7) N - N	5c	15 - 60	.0294 ± .0007	.02114 ± .0008
AVERAGES:				
1)-4) π - N	5a-5d	6 - 60	.03492 ± .00058	.02123 ± .00058
6)-7) N - N	5a, 5c	6 - 60	.02953 ± .00069	.02132 ± .00078
5)-7) N - N	5a, 5c, 5e	5 - 60	.02009 ± .00019	.01179 ± .00028

TABLE III

Fits to the difference $\sigma_{\gamma p} - \sigma_{\gamma n}$ in the region $W \geq 1.9$ GeV for various wave functions[12].

Wave Function	Form	A	B
None	$A + B\ \nu^{-1/2}$	6.6 ± 3.2	4.6 ± 5.3
Hamada-Johnston	$A + B\ \nu^{-1/2}$	1.2 ± 3.2	11.0 ± 5.3
Lomon-Feshbach	$A + B\ \nu^{-1/2}$	$.3 \pm 3.2$	9.6 ± 5.3
None	$A + B\ S^{-1/2}$	6.1 ± 3.5	7.4 ± 8.6
Hamada-Johnston	$A + B\ S^{-1/2}$	$.7 \pm 3.5$	17.5 ± 8.6
Lomon-Feshbach	$A + B\ S^{-1/2}$	$.4 \pm 3.5$	15.3 ± 8.6

FIGURE CAPTIONS

1. Impulse approximation graph. The broken line represents the incident particle of 4-momentum q, the single solid lines are the nucleons of momenta p (the interacting particle) and p_s (the spectator). The double line represents the deuteron of 4-momentum P_d.
2. Impulse approximation graph for the electron scattering case illustrating the one photon exchange; e and e' represent the initial and final electrons, respectively.
3. Graph of $\beta(S)$ versus the incident photon energy in real photoabsorption for various wave functions.
4. The difference $\sigma_{\gamma p} - \sigma_{\gamma n}$ versus incident photon energy using the Hamada-Johnston wave function.
5. A comparison of the theory to the quasielastic peak in e d scattering at 16 GeV and a scattering angle of 4°. The theory is very insensitive to the wave function.
6. (a) The ratio F_2/F_2 (smeared) versus ω for various values of q^2 using the Hamada-Johnston wave function and the ω for fit to F_2

   (b) The ratio F_2/F_2 (smeared) versus ω' for various values of q^2 using the Hamada-Johnston wave function and the ω' fit to F_2.
7. The ratio F_2/F_2 (smeared) versus ω for various wave functions.
8. The ratios $\rho = N/P$ (smeared) and $\rho' = N/P$ each plotted versus x' showing the crucial $x' \lesssim 1/4$ effect described in the text.
9. The momentum distribution $|\Phi(p_s)|$ for various wave functions.

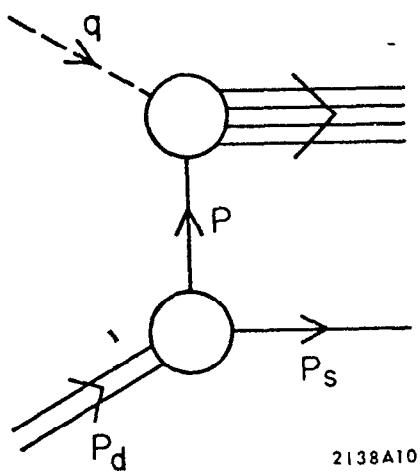

FIG. 1

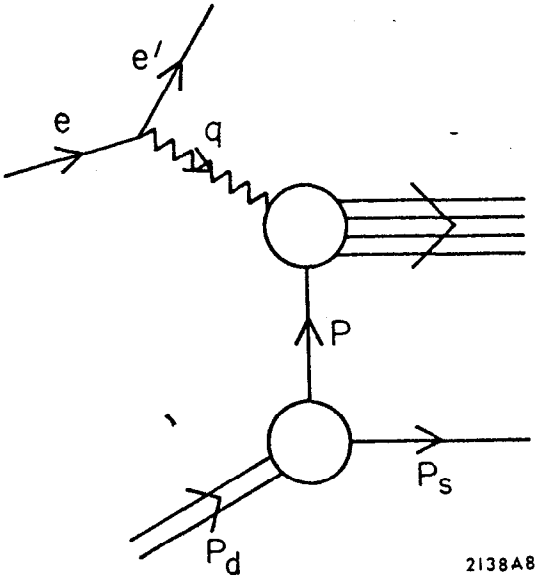

FIG. 2

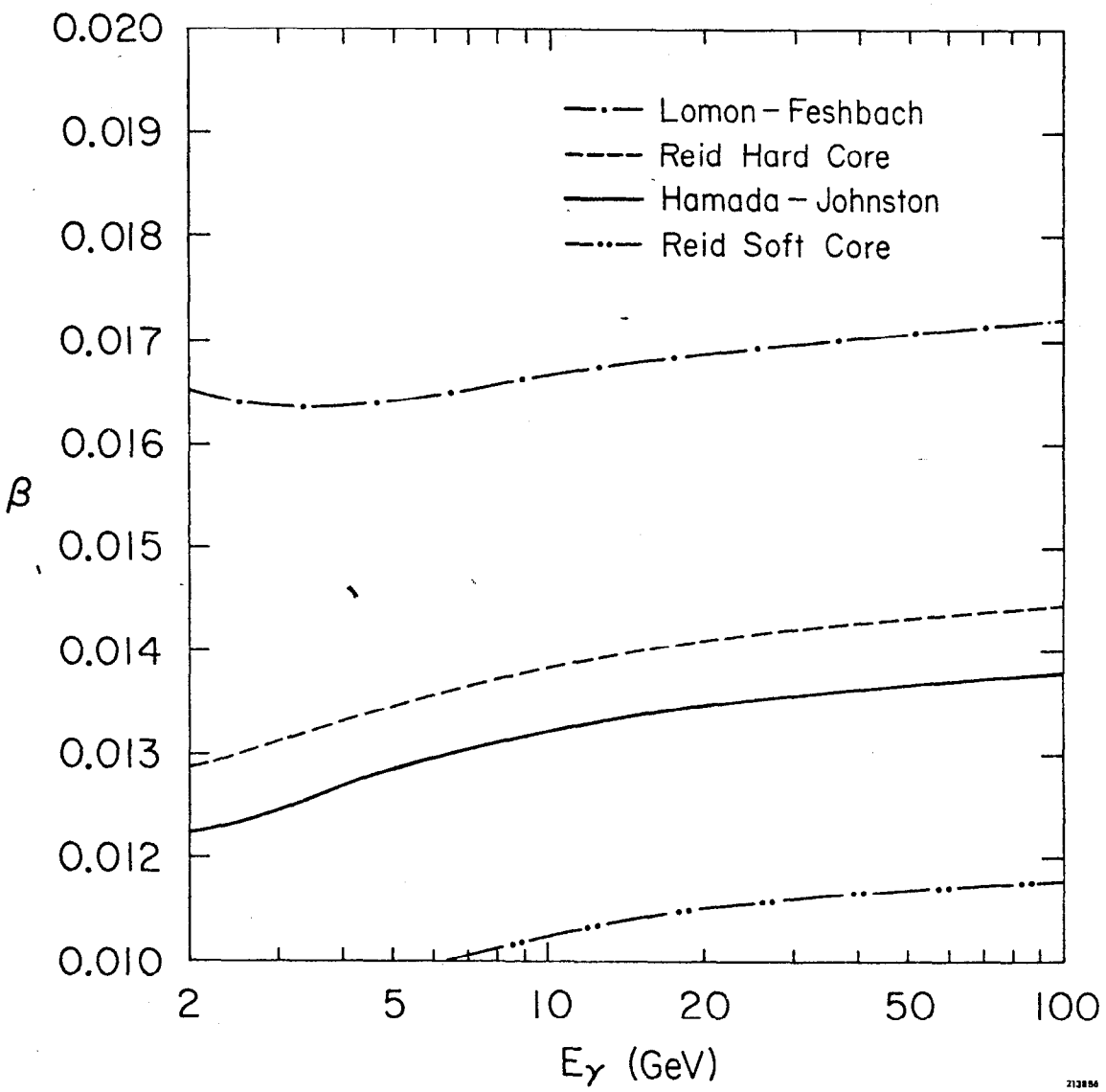
0.020
0.019
0.018
0.017
0.016
0.015
0.014
0.013
0.012
0.010
β
2
5
10
20
50
100
E_γ (GeV)
Lomon – Feshbach
Reid Hard Core
Hamada – Johnston
Reid Soft Core
213856

FIG. 3

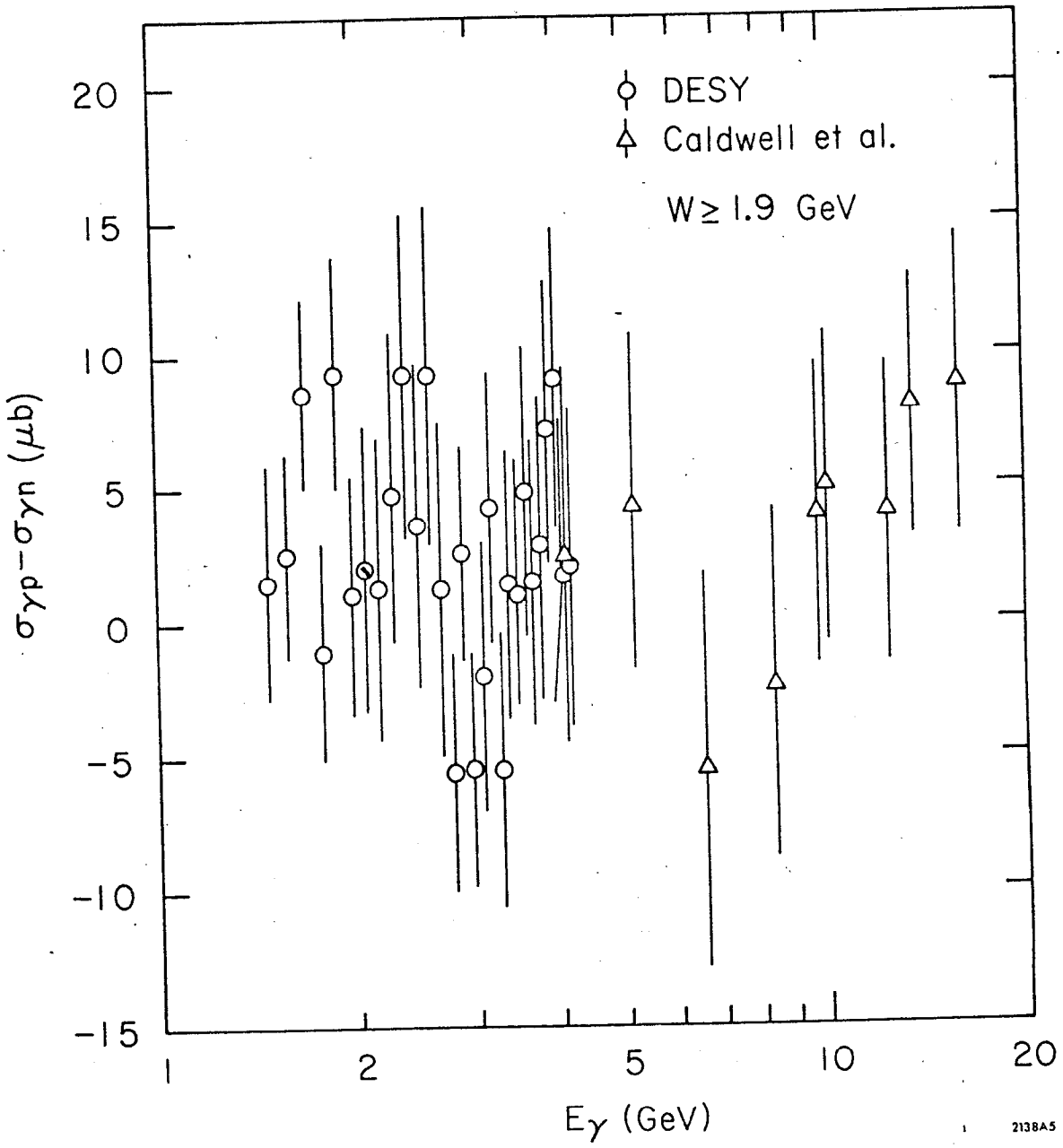
DESY
Caldwell et al.
W≥ 1.9 GeV
$\sigma_{\gamma p} - \sigma_{\gamma n}$ (μb)
E_γ (GeV)
20
15
10
5
0
-5
-10
-15
1
2
5
10
20
2138A5

Fig. 4

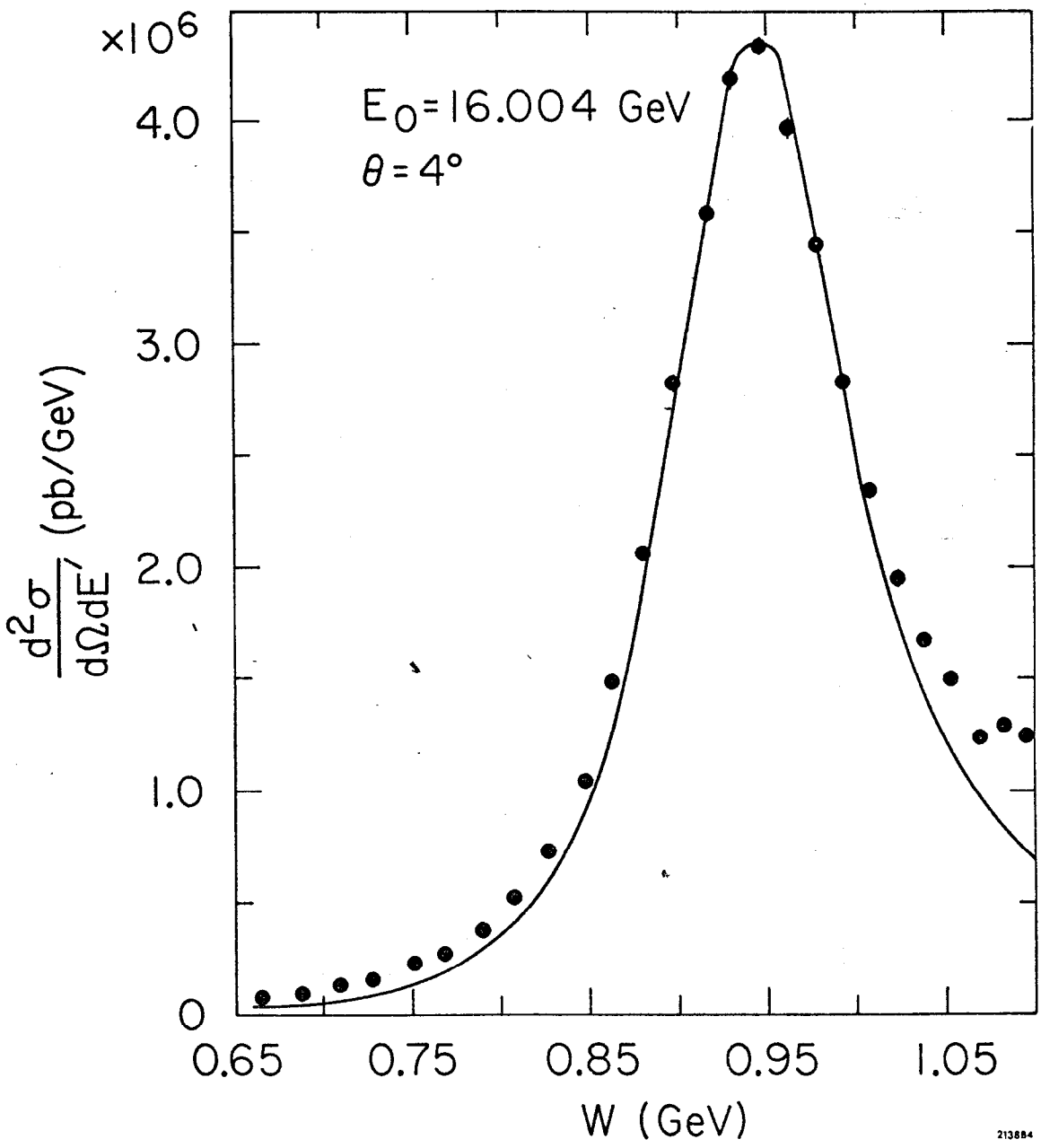
×10^6
4.0
3.0
2.0
1.0
0
E0=16.004 GeV
θ=4°
d²σ/dΩdE' (pb/GeV)
0.65
0.75
0.85
0.95
1.05
W (GeV)
213884

FIG. 5

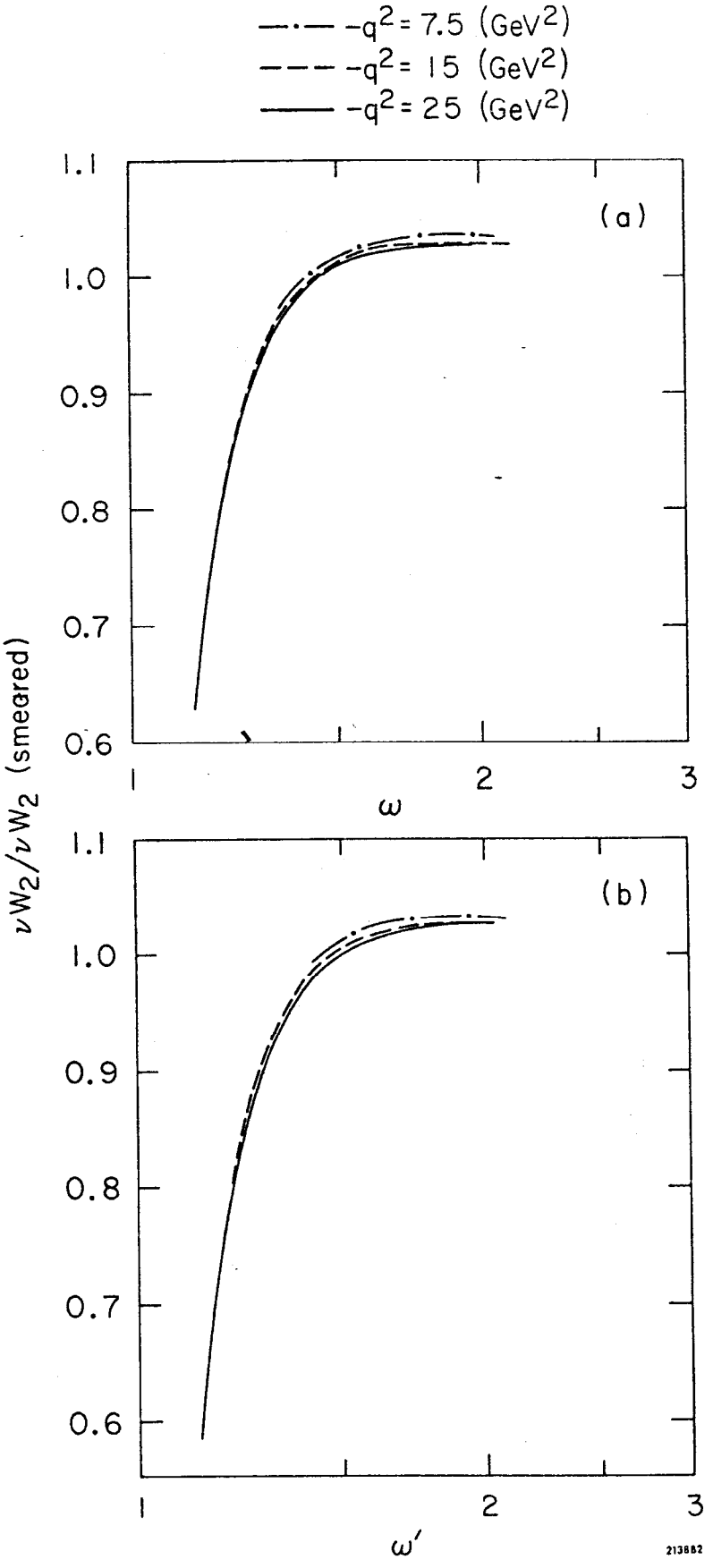
$-q^2 = 7.5$ (GeV^2)
$-q^2 = 15$ (GeV^2)
$-q^2 = 25$ (GeV^2)
(a)
(b)
$\nu W_2/\nu W_2$ (smeared)
ω
ω'
1.1
1.0
0.9
0.8
0.7
0.6
1
2
3
213882

FIG. 6

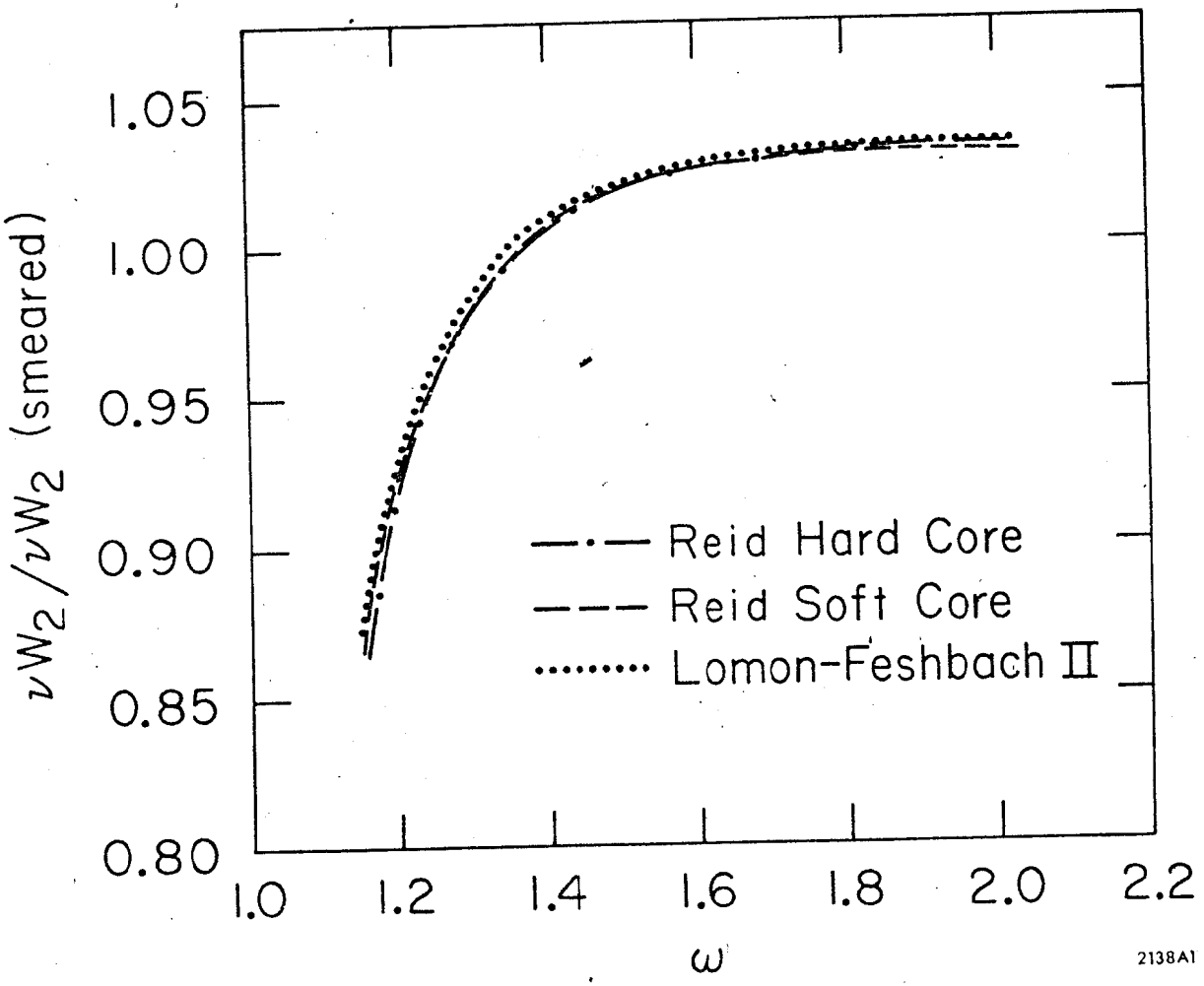
1.05
1.00
0.95
0.90
0.85
0.80
1.0
1.2
1.4
1.6
1.8
2.0
2.2
ω
νW2 /νW2 (smeared)
Reid Hard Core
Reid Soft Core
Lomon-Feshbach II
2138A1

FIG. 7

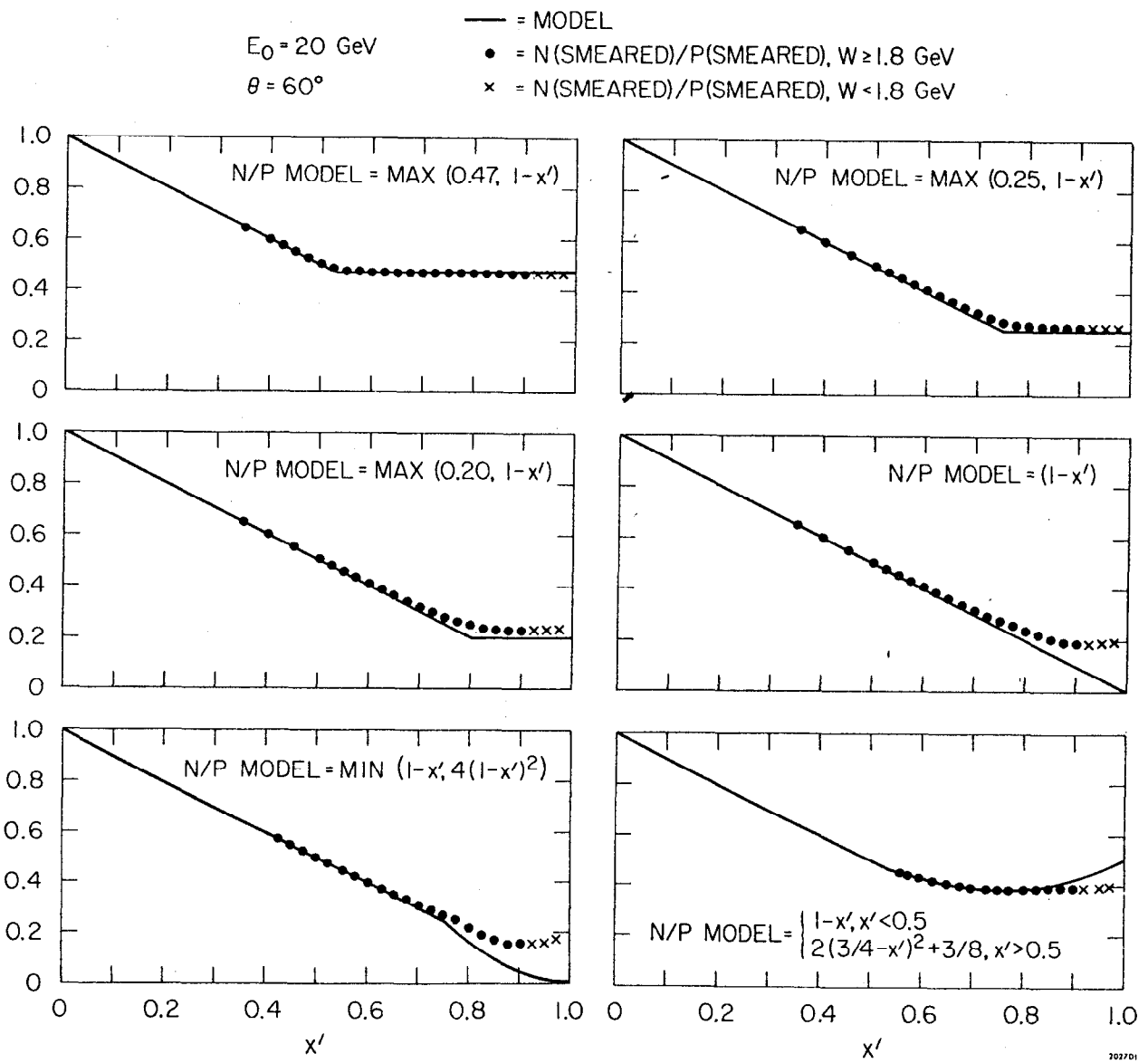
— = MODEL
E_0 = 20 GeV
θ = 60°
• = N(SMEARED)/P(SMEARED), W ≥ 1.8 GeV
× = N(SMEARED)/P(SMEARED), W < 1.8 GeV
N/P MODEL = MAX (0.47, 1-x')
N/P MODEL = MAX (0.25, 1-x')
N/P MODEL = MAX (0.20, 1-x')
N/P MODEL = (1-x')
N/P MODEL = MIN (1-x', 4(1-x')²)
N/P MODEL = 1-x', x'<0.5
2(3/4-x')²+3/8, x'>0.5
0
0.2
0.4
0.6
0.8
1.0
x'
702701

FIG. 8

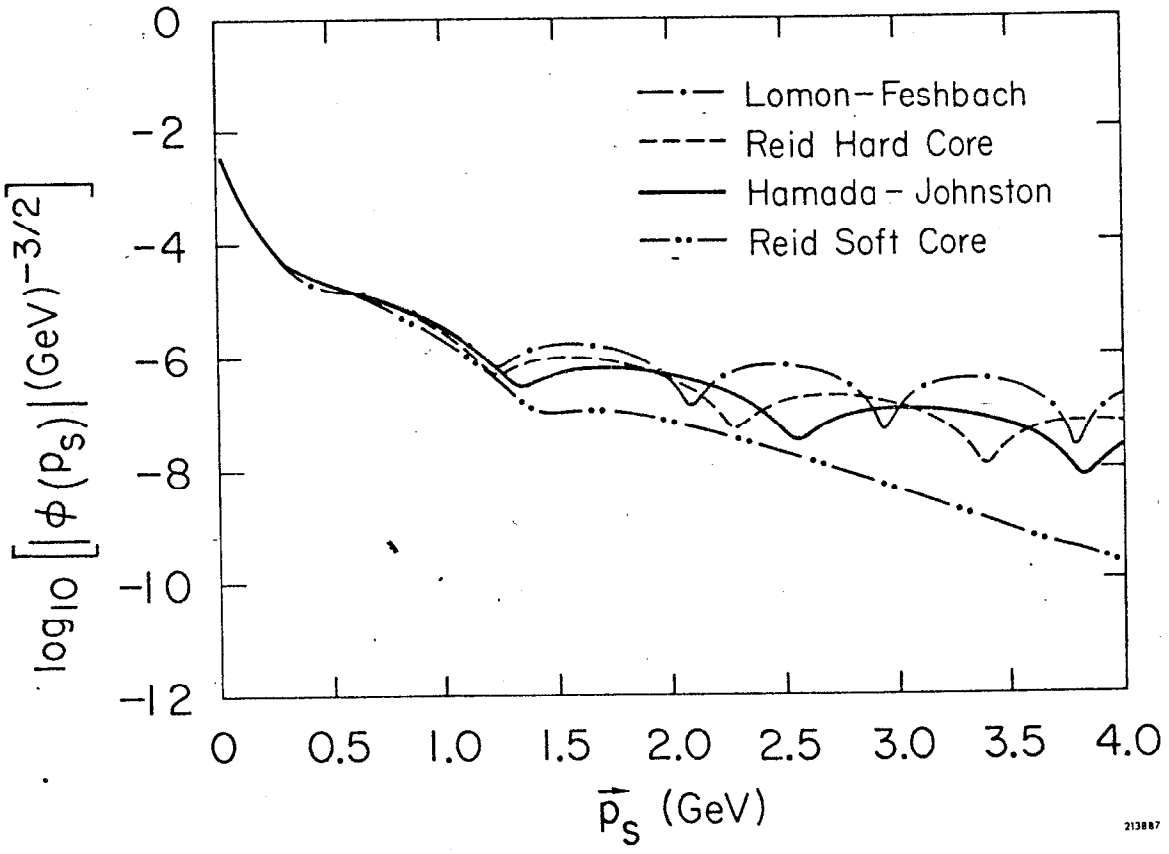
Lomon-Feshbach
Reid Hard Core
Hamada-Johnston
Reid Soft Core
$\log_{10}\left[|\phi(p_s)|^{(GeV)^{-3/2}}\right]$
$\vec{p}_s$ (GeV)
0
-2
-4
-6
-8
-10
-12
0
0.5
1.0
1.5
2.0
2.5
3.0
3.5
4.0
213887

FIG. 9